FEASIBILITY STUDY

# Laser Doppler velocimetry momentum defect measurements of cable drag at low to moderate Reynolds numbers.

*by*

Paul E. Dimotakis

Naval Construction Battalion Center

Contract No. N62583/77 - M - R541

*Altadena, California*

*August 1977*

# ABSTRACT

The problem of measuring cable drag coefficients at low to moderate Reynolds numbers ($100 < Re < 30{,}000$) is addressed and alternative methods of measurement are analyzed. The very low forces and pressures involved at the lower Reynolds numbers render conventional measurement methods less suitable candidates. Laser Doppler velocity measurements, however, of the momentum defect in the wake appear capable of yielding sufficient accuracy ($< \pm 5\%$) in the determination of the drag coefficient. This conclusion assumes that a test facility can be utilized with a sufficiently uniform flow field, low turbulence level and a free stream velocity which either remains stable during the wake survey measurement time interval or can be monitored independently. Water and air appear as almost equal in their merits as working fluids, with water slightly preferable as not requiring scattering particle seeding.

# I. Conventional measurements of cable drag at low to moderate Reynolds numbers

## 1. Force measurements

Direct force measurements of the drag of cables at low Reynolds number become very difficult because the forces per unit span can be very small. The situation is illustrated by the behavior of the circular cylinder, whose drag coefficient

$$c_D \equiv \frac{D/b}{\frac{1}{2} \rho U_\infty^2 d} , \qquad (1)$$

where

D : drag

b : cylinder span

$\rho$ : fluid density

$U_\infty$ : fluid velocity at infinity

d : cylinder diameter,

is dominated by the vortex shedding mechanism and *very nearly Reynolds number independent,* for a very large range of Reynolds numbers. In fact, as can be seen from figure 1,

$$0.9 < c_D < 1.5 \qquad (2a)$$

for

$$40 < Re < 2\times10^5 , \qquad (2b)$$

where Re is the Reynolds number based on the cylinder diameter and $U_\infty$

and given by

$$Re \equiv \frac{U_\infty \, d}{\nu} \, , \tag{3}$$

where

$U_\infty$ : fluid velocity at infinity

$d$ : cylinder diameter

$\nu$ : kinematic viscosity ($\equiv \mu/\rho$)

$\mu$ : absolute viscosity

$\rho$ : fluid density.

Surprisingly enough, the drag of a cylinder *for a given Reynolds number* is not all that different in air and water. From equation 1 we have,

$$D/b = \frac{c_D}{2} \rho \, U_\infty^2 \, d \, .$$

Substituting from equation 3, we have

$$U_\infty = \frac{\nu \, Re}{d} \, ,$$

and consequently,

$$D/b = \frac{c_D}{2} \left( \frac{Re^2}{d} \right) \rho \nu^2 . \tag{4}$$

The ratio of the quantity $\rho\nu^2$ for water and air is given by (see Appendix 1),

$$\frac{(\rho\nu^2)_{water}}{(\rho\nu^2)_{air}} = 3.30 \tag{5}$$

at 22°C and 1 Atm.

The drag per unit span of a 1 cm (0.394 in) cylinder is plotted in dimensional units in figure 2, as a function of Reynolds number, assuming a constant drag coefficient of $c_D \sim 1.2$. It can be seen that the forces, at the lower Reynolds numbers, are extremely small. It should also be pointed out that the dependence of the drag *for a given Reynolds number*, on the reciprocal of the cylinder diameter should be interpreted with some care (equation 4). In any practical situation, a cylinder that is too small will pose measurement problems. This becomes clear if one takes into account the tare drag of the supporting structure or metric sections of the tunnel. Closely tied with this problem is the difficulty of providing truly sectional estimates of the drag per unit span of the cable, when making direct force measurements at low Reynolds number.

## 2. Pressure measurements

It is also possible to measure the drag on a cylinder-like structure by making pressure measurements along its perimetry yielding data of $p(\phi) - p_\infty$ on the body surface. The drag per unit span can

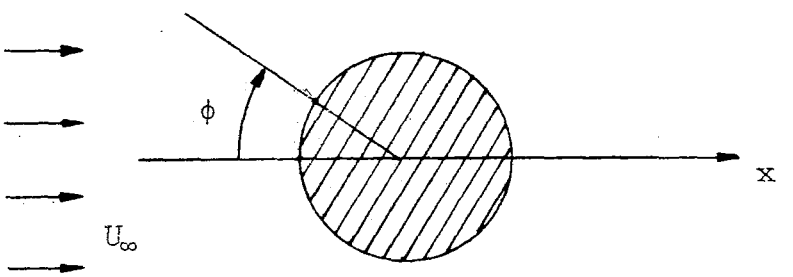


then be estimated by integrating the data numerically (neglecting viscous forces) to obtain,

$$D/b = d \int_0^{\pi} [p(\phi) - p_\infty] \cos\phi d\phi \ . \qquad (6)$$

One major advantage of this technique is that it allows *truly sectional measurements* of the drag, free of end effects due to the supporting structures.

The pressure difference,

$$\Delta p \equiv p - p_\infty \ , \qquad (7)$$

is usually normalized by $\frac{1}{2} \rho U_\infty^2$ to yield the pressure coefficient

$$c_p \equiv \frac{p - p_\infty}{\frac{1}{2} \rho U_\infty^2} \ . \qquad (8)$$

It can be shown theoretically and verified experimentally that the pressure coefficient, in this case, is of the order of unity, i.e.

$$|c_p| \lesssim 1 \ . \qquad (9)$$

Consequently, to measure the drag per unit span of a cylinder, requires measuring pressure differences of the order of

$$p - p_\infty \sim \frac{1}{2} \rho U_\infty^2 \ ,$$

or, for a given Reynolds number,

$$p - p_\infty \sim \frac{1}{2} \left(\frac{Re^2}{d^2}\right) \rho\nu^2 \ . \qquad (10)$$

It may again be a surprising result that, *for a given Reynolds number*, the pressure differences in air and water are about the same (see equation 5). The right hand side of equation 10 is plotted in

dimensional units in figure 3 as a function of Reynolds number, for a cylinder of $d = 1.0$ cm . It can be seen that the pressures at low Reynolds numbers (see Appendix 1.3) are very low indeed. Nevertheless, modern electronic manometers are capable of accurate measurements down to $10^{-3}$ - $10^{-4}$ mm Hg and would be suitable for the measurements in air. Such a scheme might be a viable possibility *if the cost of instrumenting the cables with pressure taps, in every case, is not prohibitive.*

## II. Momentum defect measurements of cable drag at low to moderate Reynolds numbers

### 1. Theoretical considerations

Consider a fluid moving uniformly at infinity, with a velocity $U_\infty$ in the x direction, and a cylinder - like body on the z - axis. Consider also a contour A B C D E F G H on the $z = 0$ plane around the body, as shown in the sketch.

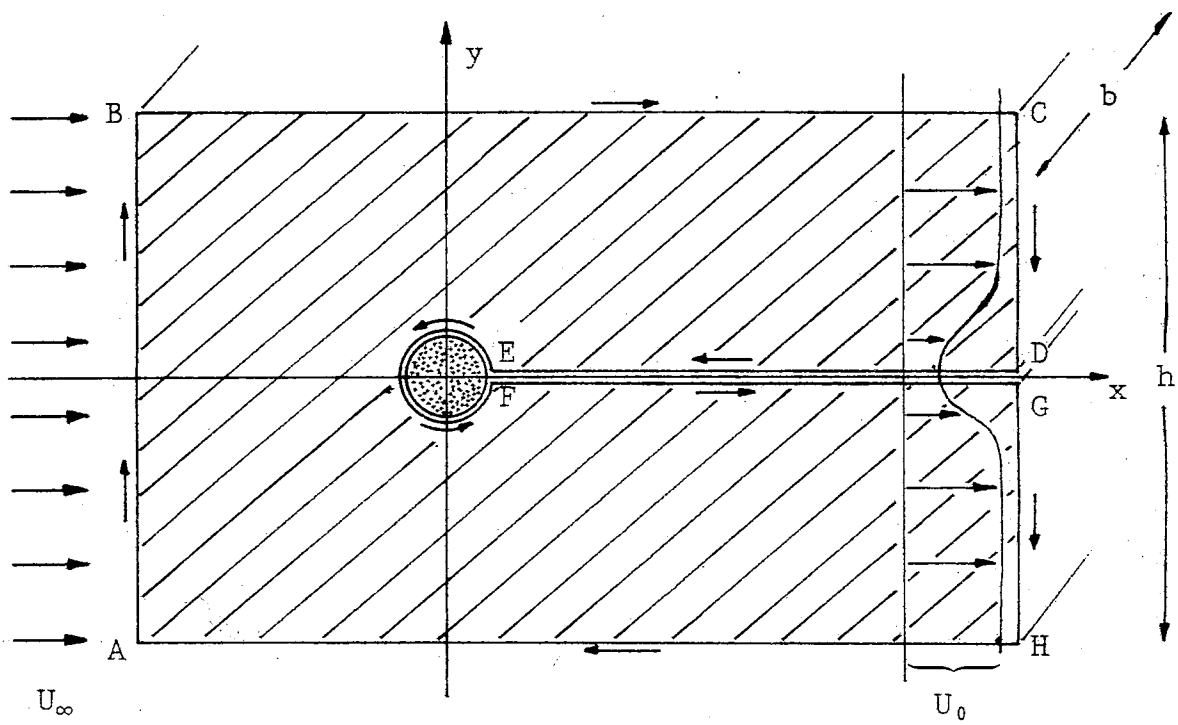


From the momentum equation, we have,

$$\frac{\partial}{\partial t}\,\underline{u} + \nabla\cdot\underline{u}\,\underline{u} + \frac{1}{\rho}(\nabla p - \nabla\cdot\underline{\tau}) = 0\,, \qquad (11)$$

where (summation is implied over repeated indices)

$$\nabla \equiv \hat{e}_k \frac{\partial}{\partial x_k} \equiv \hat{e}_x \frac{\partial}{\partial x} + \hat{e}_y \frac{\partial}{\partial y} + \hat{e}_z \frac{\partial}{\partial z} \tag{12}$$

is the gradient operator,

$$\underline{u} = \hat{e}_i u_i = \hat{e}_x u + \hat{e}_y v + \hat{e}_z w \tag{13}$$

is the velocity vector and $\underline{\underline{\tau}}$ is the viscous stress tensor, given for incompressible flow by,

$$\underline{\underline{\tau}} = \hat{e}_i \hat{e}_j \mu \left( \frac{\partial u_i}{\partial x_j} + \frac{\partial u_j}{\partial x_i} \right) , \tag{14}$$

where $\mu$ is the absolute viscosity.

Consider now a rectangular volume $V$ of span $b$ along the $z$ - axis, whose $z = 0$ intercept is the interior of the contour A B C D E F G H , and integrate the momentum equation 11 in the interior of the volume. This yields,

$$\int_V \left[ \frac{\partial}{\partial t} \underline{u} + \nabla \cdot \underline{u}\,\underline{u} + \frac{1}{\rho} (\nabla p - \nabla \cdot \underline{\underline{\tau}}) \right] dV = 0 \tag{15}$$

or, using Gauss' theorem and choosing the pressure at infinity as the origin in pressure, we have

$$\frac{\partial}{\partial t} \int_V \underline{u}\, dV + \int_S \underline{u}\,\underline{u} \cdot d\underline{S} + \frac{1}{\rho} \int_S (p - p_\infty)\, d\underline{S} - \frac{1}{\rho} \int_S \underline{\underline{\tau}} \cdot d\underline{S} = 0 \tag{16}$$

where $d\underline{S}$ is a vector directed along the outward normal, of magnitude equal to the surface element $dS$ , i.e.

$$d\underline{S} \equiv \hat{e}_i \, dS_i = \hat{e}_x \, dS_x + \hat{e}_y \, dS_y + \hat{e}_z \, dS_z \, . \qquad (17)$$

We now take the x - component of equation 16 to obtain

$$\frac{\partial}{\partial t}\int_V \hat{e}_x \cdot \underline{u} \, dV + \int_S \hat{e}_x \cdot \underline{u}\,\underline{u} \cdot d\underline{S} + \frac{1}{\rho}\int_S (p - p_\infty)\hat{e}_x \cdot d\underline{S} - \frac{1}{\rho}\int_S \hat{e}_x \cdot \underline{\tau} \cdot d\underline{S} = 0$$

or

$$\frac{\partial}{\partial t}\int_V u \, dV + \int_S u \, u_i dS_i + \frac{1}{\rho}\int_S (p - p_\infty) \, dS_x$$

$$- \nu \int_S \left( \frac{\partial u}{\partial x_i} + \frac{\partial u_i}{\partial x} \right) dS_i = 0 \qquad (18)$$

where $\nu \equiv \mu / \rho$ is the kinematic viscosity and summation over repeated indices is implied.

Consider now the time average of equation 18. The first integral vanishes and we are left with,

$$\int_S \overline{u\,u_i} \, dS_i + \frac{1}{\rho}\int_S (\overline{p} - p_\infty) \, dS_x - \nu \int_S \left( \frac{\partial \overline{u}}{\partial x_i} + \frac{\partial \overline{u_i}}{\partial x} \right) dS_i = 0, \qquad (19)$$

Each of the surface integrals can be computed as the sum of integrals over each section, i.e.

$$\int_S = \int_{AB} + \int_{BC} + \int_{CD} + \int_{DE} + \int_{EF} + \int_{FG} + \int_{GH} + \int_{HA} = 0$$

Note that the contributions from the two integrals D E and F G cancel, if we choose the distance $\overline{FE}$ to be infinitesimally small,

and that *minus the integral E F is equal to the drag divided by the fluid density.* Consequently,

$$D/\rho = -\int_{EF} = \int_{AB} + \int_{BC} + \int_{CH} + \int_{HA} . \qquad (20)$$

If we now choose the edges of the surface to be sufficiently far away from the body all mean velocity gradients can be neglected and we have,

$$D/\rho = \int_{AB} \overline{u^2}\, dy\, dz + \int_{BC} \overline{uv}\, dx\, dz + \int_{CH} \overline{u^2}\, dy\, dz + \int_{HA} \overline{uv}\, dx\, dz + \frac{1}{\rho}\int_{AB} (\overline{p} - p_\infty)\, dy\, dz + \frac{1}{\rho}\int_{CH} (\overline{p} - p_\infty)\, dy\, dz . \qquad (21)$$

Dividing equation 21 by $\frac{1}{2} U_\infty^2\, bd$, we have

$$c_D \equiv \frac{D/b}{\frac{1}{2}\rho U_\infty^2 d} = 2\left\{\int_{AB} + \int_{CH}\right\} \frac{\overline{u^2}}{U_\infty^2}\, d\eta\, d\zeta + 2\left\{\int_{BC} + \int_{HA}\right\} \frac{\overline{uv}}{U_\infty^2}\, d\xi\, d\zeta + \left\{\int_{AB} + \int_{CH}\right\} \overline{c_p}\, d\eta\, d\zeta , \qquad (22)$$

where $\overline{c_p}$ is the (time averaged) pressure coefficient

$$\overline{c_p} = \frac{\overline{p} - p_\infty}{\frac{1}{2}\rho U_\infty^2} , \qquad (23)$$

and $\xi = x/d$, $\eta = y/d$, $\zeta = z/b$ are the normalized dimensionless coordinates.

We can use the continuity equation, for an incompressible fluid,

$$\nabla \cdot \underline{u} = 0 \tag{24}$$

integrated over the volume V

$$\int_V \nabla \cdot \underline{u} \, dV \equiv \int_S \underline{u} \cdot d\underline{S} = 0 \ , \tag{25}$$

to rewrite equation 22. Multiplying equation 25 with $2/U_\infty$ and subtracting it from equation 22 yields,

$$c_D = 2\left\{\int_{AB} + \int_{CH}\right\} \frac{\overline{u^2} - U_\infty \bar{u}}{U_\infty^2} \, d\eta \, d\zeta$$

$$+ 2\left\{\int_{BC} + \int_{HA}\right\} \frac{\overline{uv} - U_\infty \bar{v}}{U_\infty^2} \, d\xi \, d\zeta \tag{26}$$

$$+ \left\{\int_{AB} + \int_{CH}\right\} \overline{c_p} \, d\eta \, d\zeta \ .$$

## 2. Assumptions and simplifications

a. Upstream conditions. In practice, we can usually place the upstream edge A B of the integration surface sufficiently far from the body for the conditions to be essentially equal to the conditions at

infinity, i.e. $\underline{u} \simeq \hat{e}_x U_\infty$ and $p \simeq p_\infty$. In that case, we have

$$\int_{AB} \frac{\overline{u^2} - U_\infty \overline{u}}{U_\infty^2} \, d\eta \, d\zeta = 0 \tag{27}$$

and

$$\int_{AB} \overline{c_p} \cdot d\eta \, d\zeta = 0 \, . \tag{28}$$

Let us now decompose the velocity into its mean value and fluctuating part, i.e.

$$u = \overline{u} + u' \tag{29a}$$

and

$$v = \overline{v} + v' \, . \tag{29b}$$

We then have,

$$\overline{u^2} = \overline{u}^2 + \overline{u'^2} \tag{30}$$

and

$$\overline{uv} = \overline{u}\,\overline{v} + \overline{u'v'} \, . \tag{31}$$

The product $\overline{uv}$ appears only in the integrals B C and H A whose paths can be chosen well outside the region where fluctuations occur. In that case, the Reynolds stress $\overline{u'v'}$ is zero along those two paths of integration and, consequently, $\overline{uv} \simeq \overline{u}\,\overline{v}$ there. With these substitutions and simplifications we have,

$$c_D \simeq 2 \int_{HC} \frac{\bar{u}}{U_\infty} \left( 1 - \frac{\bar{u}}{U_\infty} \right) d\eta\, d\zeta - 2 \int_{HC} \frac{\overline{u'^2}}{U_\infty^2} d\eta\, d\zeta - \int_{HC} \overline{c_p}\, d\eta\, d\zeta$$

$$+ 2 \left\{ \int_{AH} + \int_{CB} \right\} \frac{\bar{v}}{U_\infty} \left( 1 - \frac{\bar{u}}{U_\infty} \right) d\xi\, d\zeta \,, \qquad (32)$$

where the directions of integrations have been reversed.

b. Finite test section effects. For measurements performed in test sections with top and bottom walls that can be set for zero pressure gradient (constant velocity) in the absence of any blockage, it is possible to align everything so that there is no perpendicular velocity component along the top and bottom edges of the rectangular measurement contour.

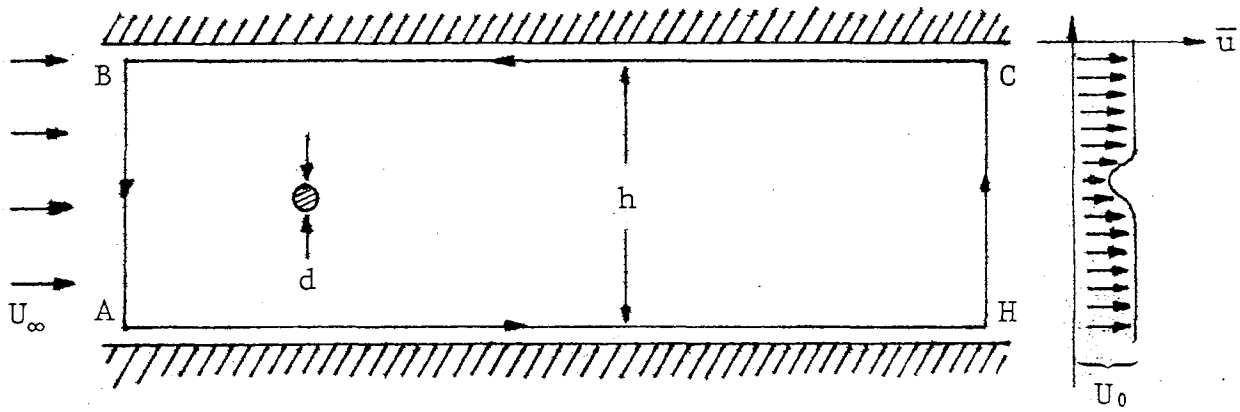


In that case, the integrals along A H and C B , in equation 32, will vanish since $v = 0$ along the path of integration.

It is possible to use the fact that there is no mass flux through B C and A H to simplify some of the expressions. In particular, define $\delta_1$ , the displacement thickness, at the downstream contour C H , such that

$$b(h - \delta_1)U_o \equiv \int_{HC} \bar{u}\, dy\, dz$$

r

$$\delta_1 \equiv d \int_{HC} \left(1 - \frac{\bar{u}}{U_o}\right) d\eta\, d\zeta, \tag{33}$$

where $U_o$ is the velocity at the downstream station outside the wake. Since we have assumed that there is no mass flux through the top and bottom edges of the contour, we have

$$h\, U_\infty = (h - \delta_1)\, U_o$$

and therefore,

$$\frac{U_o}{U_\infty} = \frac{1}{1 - \delta_1/h} . \tag{34}$$

c. The pressure coefficient. We can separate the effects of free stream acceleration due to the displacement thickness (equation 34), from pressure differences across the wake, namely

$$\overline{c_p} \equiv \frac{\bar{p} - p_\infty}{\frac{1}{2}\rho U_\infty^2} = \frac{p_o - p_\infty}{\frac{1}{2}\rho U_\infty^2} + \frac{\bar{p} - p_o}{\frac{1}{2}\rho U_\infty^2} \equiv c_{p_o} + \overline{c_{p_w}} .$$

We can now use Bernoulli's equation, which is applicable outside the wake, to compute $c_{p_o}$. This yields

$$p_o + \tfrac{1}{2}\rho U_o^2 = p_\infty + \tfrac{1}{2}\rho U_\infty^2 ,$$

and therefore,

$$c_{p_o} \equiv \frac{p_o - p_\infty}{\frac{1}{2}\rho U_\infty^2} = 1 - \frac{U_o^2}{U_\infty^2} \tag{35}$$

or, using equation 34,

$$c_{p_o} = -\frac{\delta_1}{h} \times \frac{(2 - \delta_1/h)}{(1 - \delta_1/h)^2} \ . \tag{36}$$

To compute the pressure coefficient across the wake, i.e.

$$\overline{c_{p_w}} \equiv \frac{\overline{p} - p_o}{\frac{1}{2}\rho U_\infty^2} \ , \tag{37}$$

consider the y-component of the momentum equation (11) in the far wake $(x/d >> 1)$. Taking the time average and neglecting viscous forces, we have

$$\frac{\partial}{\partial x}\overline{uv}^t + \frac{\partial}{\partial y}\overline{v^2}^t + \frac{\partial}{\partial z}\overline{uw}^t \simeq -\frac{1}{\rho}\frac{\partial}{\partial y}\overline{p}^t \ . \tag{38}$$

If the body has spanwise variations, the $\partial/\partial z$ derivative need not be zero even in the far wake (streamwise vortices are possible). We can average once again, however, in the spanwise direction to obtain

$$\frac{\partial}{\partial x}\overline{uv}^{t,z} + \frac{\partial}{\partial y}\overline{v^2}^{t,z} \simeq -\frac{1}{\rho}\frac{\partial}{\partial y}\overline{p}^{t,z} \ . \tag{39}$$

To a good approximation in the far wake, we can neglect the first term (Townsend 1976) to obtain

$$\frac{\partial}{\partial y}\left(\frac{1}{\rho}\,\overline{p} + \overline{v^2}\right) \simeq 0$$

where the averaging superscripts are implied. Integrating with respect to y, we have

$$\frac{1}{\rho}\,(\overline{p} - p_o) \simeq -\overline{v^2} \tag{40}$$

Consequently, the pressure coefficient across the wake becomes

$$\overline{c_{p_w}} \equiv \frac{\overline{p} - p_o}{\frac{1}{2}\rho U_\infty^2} \simeq -2\,\frac{\overline{v^2}}{U_\infty^2} \tag{41}$$

d. The drag coefficient in terms of downstream quantities. Using equations 32, 34, 36 and 41 we have, after a little algebra,

$$c_D \simeq \frac{2}{(1 - \delta_1/h)^2}\left\{\int_{HC}\frac{\overline{u}}{U_o}\left(1 - \frac{\overline{u}}{U_o}\right)d\eta\,d\zeta - \int_{HC}\frac{\overline{u'^2} - \overline{v^2}}{U_o^2}\,d\eta\,d\zeta + \frac{\delta_1^2}{2hd}\right\} \tag{42}$$

The displacement thickness $\delta_1$ can be estimated as follows. From equation 33 we have

$$\frac{\delta_1}{d} = \int_{HC}\left(1 - \frac{\overline{u}}{U_o}\right)d\eta\,d\zeta \sim \int_{HC}\frac{\overline{u}}{U_o}\left(1 - \frac{\overline{u}}{U_o}\right)d\eta\,d\zeta$$

for large $x/d$ as $\overline{u}/U_o \to 1$. But, neglecting terms of order $\delta_1/h$ and the integral over the velocity fluctuations, we have

$$c_D \sim 2\int_{HC'}\frac{\overline{u}}{U_o}\left(1 - \frac{\overline{u}}{U_o}\right)d\eta\,d\zeta$$

and therefore $\delta_1 / d \sim c_D/2$ .

For wide test sections $\delta_1/h \to 0$ and equation 42 reduces to

$$c_D \simeq 2 \int_{HC} \frac{\bar{u}}{U_o}\left(1 - \frac{\bar{u}}{U_o}\right) d\eta\, d\zeta - \int_{HC} \frac{\overline{u'^2} - \overline{v^2}}{U_o^2}\, d\eta\, d\zeta \,. \qquad (43)$$

e. The integral over the velocity fluctuations. The contribution from the integral over the velocity fluctuations decreases in the far wake, as $x/d \to \infty$ . This can be shown by the following argument. The velocity profile in the far wake is approximately similar, i.e.

$$\bar{u}(x,y) \simeq U_o - u_o(x)\, f\left[y/a(x)\right], \qquad (44)$$

where $u_o(x)$ is the velocity defect on the centerline, and $a(x)$ is the wake half width, i.e.

$$f(1) = \tfrac{1}{2}. \qquad (45)$$

To a good approximation, in fact (Townsend 1976),

$$f(y/a) \simeq e^{-\ln 2\, y^2/a^2} . \qquad (46)$$

We can normalize $a(x)$, the wake half width, with the body diameter, to define a dimensionless wake half width,

$$\alpha(x) \equiv \frac{a(x)}{d} \qquad (47)$$

and express the velocity profile in terms of the dimensionless coordi-

nate $\eta \equiv y/d$, i.e.

$$\overline{u} \simeq U_o - u_o(x)\ f(\eta/\alpha) \tag{48}$$

Under the same basic assumptions, we should also expect the velocity fluctuation profiles $\overline{u'^2}$ and $\overline{v'^2}$ to be approximated by

$$\overline{u'^2} \simeq c_1^2\, u_0^2(x)\, g_1(\eta/\alpha) \tag{49a}$$

and

$$\overline{v^2} \simeq \overline{v'^2} \simeq c_2^2\, u_0^2\,(x)\ g_2(\eta/\alpha) \tag{49b}$$

where $c_1$ and $c_2$ are constants. Consequently we have

$$\int_{HC} \frac{\overline{u'^2} - \overline{v^2}}{U_0^2}\, d\eta \simeq \frac{u_0^2}{U_0^2} \int_{HC} \left[c_1^2\, g_1^2\,(\eta/\alpha) - c_2^2\, g_2^2(\eta/\alpha)\right]\, d\eta \tag{50}$$

$$= \frac{\alpha(x)\, u_0^2(x)}{U_0^2} \int_{HC} \left[c_1^2\, g_1^2\,(\eta') - c_2^2\, g_2^2\,(\eta')\right] d\eta'.$$

For a two dimensional wake we find (e.g. Townsend 1976) that

$$\alpha(x)\ u_0(x) \simeq \text{const.} \tag{51}$$

and, in particular

$$u_0(x)/U_0 \propto \left(\frac{x - x_0}{d}\right)^{-\frac{1}{2}} \tag{52}$$

and

$$\alpha(x) \propto \left( \frac{x - x_0}{d} \right)^{\frac{1}{2}} . \tag{53}$$

Consequently, we have

$$\int_{HC} \frac{\overline{u'^2} - \overline{v^2}}{U_0^2} \, d\eta \propto \text{const.} \left( \frac{x - x_0}{d} \right)^{-\frac{1}{2}} . \tag{54}$$

## III. Measurement procedure

From equation 42, it can be seen that the drag coefficient $c_D$ can be estimated from measurements across the wake, at some downstream location $x_1$, such that $x_1/d$ is large enough for equation 41 to be valid. *If there are no spanwise variations in the body to be measured, it is sufficient to measure at one spanwise location* $z_1$, *the following quantities:*

$$\left.\begin{array}{ll} \text{(i)} & \bar{u}(x_1, y, z_1) \\ \text{(ii)} & \overline{u'^2}(x_1, y, z_1) \\ \text{(iii)} & \overline{v^2}(x_1, y, z_1) \end{array}\right\} \quad -h/2 < y < h/2$$

in order to evaluate $\delta_1$ (equation 33)

$$\delta_1 = \int_{-h/2}^{h/2} \left(1 - \frac{\bar{u}}{U_0}\right) dy \,, \tag{56}$$

and $c_D$ (equation 42)

$$c_D \simeq \frac{2}{(1 - \delta_1/h)^2} \left\{ \int_{-h/2d}^{h/2d} \left[ \frac{\bar{u}}{U_0} \left(1 - \frac{\bar{u}}{U_0}\right) - \frac{\overline{u'^2} - \overline{v^2}}{U_0^2} \right] d\eta + \frac{\delta_1^2}{2hd} \right\}, \tag{57}$$

where $\eta = y/d$ .

*If there are spanwise variations in the body* (e.g. twisted cable) *it is necessary to measure at several locations* $z$ *within the spanwise period* $b$, i.e.

$$\left.\begin{array}{ll} \text{(i)} & \overline{u}(x_1, y, z) \\ \text{(ii)} & \overline{u'^2}(x_1, y, z) \\ \text{(iii)} & \overline{v^2}(x_1, y, z) \end{array}\right\} \quad \left\{\begin{array}{l} -h/2 < y < h/2 \\ -b/2 < z < b/2 \end{array}\right.$$

*and use the full equations 33 and 42.*

It should be possible to improve the accuracy of the measurement of the drag coefficient $c_D$, as computed from the data on the basis of equation 42 or 57, and also estimate the confidence level for the measurement, by measuring at several downstream stations.

## IV. Measurement specifications

### 1. Velocity measurement requirements

The very small percentage defects in the two dimensional wake at large $x/d$ necessitate extremely accurate velocity measurements. Using equation 48 we have, at large $x/d$ ,

$$c_D \simeq 2 \frac{u_0(x)}{U_0} \int f(\eta/\alpha) \left[ 1 - \frac{u_0(x)}{U_0} f(\eta/\alpha) \right] d\eta \qquad (58)$$

or, to first order in $u_0(x)/U_0$ ,

$$c_D \sim \frac{2\,\alpha(x)\,u_0(x)}{U_0} \int_{-\infty}^{\infty} f(\eta')\, d\eta' \quad . \qquad (59)$$

Using the empirical form for $f(\eta')$, as given by equation 46, we have

$$\int_{-\infty}^{\infty} f(\eta')\, d\eta' \sim \left( \frac{\pi}{\ln 2} \right)^{\frac{1}{2}} \simeq 2.13 \qquad (60)$$

and therefore

$$\frac{u_0(x)}{U_0} \sim 0.235 \frac{c_D}{\alpha(x)} \quad . \qquad (61)$$

We can use an empirical estimate for the wake width $\alpha(x)$ , given by (Schlichting 1968),

$$\alpha(x) \sim \tfrac{1}{4} \left( c_D \frac{x - x_0}{d} \right)^{\frac{1}{2}} , \qquad (62)$$

to obtain an estimate for the centerline velocity defect $u_0(x)$ . Substituting equation 62 into 61 yields

$$\frac{u_0(x)}{U_0} \sim 0.94 \left( \frac{x - x_0}{c_D d} \right)^{-\frac{1}{2}} . \qquad (63)$$

It can be seen that at large $x/d$ the velocity defect $u_0(x)$ is only a few percent of the local free stream velocity $U_0$ . Consequently, accuracies of fractions of a percent are required to measure the quantities of interest. This is dictated by the requirement that the edges of the wake be accurately determined to permit a reliable evaluation of the necessary integrals. The required accuracies, as can be deduced from equation 63, will be a function of $x/d$ . Generally speaking, however, measurement accuracies, for the three quantities of interest, namely $\overline{u}$ , $\overline{u'^2}$ and $\overline{v^2}$ , should be of the order of

$$\frac{\delta \overline{u}}{U_0} \sim \pm 0.05\% \quad , \qquad (64a)$$

$$\frac{\delta (\overline{u'^2})^{\frac{1}{2}}}{U_0} \sim \pm 1\% \quad , \qquad (64b)$$

and

$$\frac{\delta (\overline{v^2})^{\frac{1}{2}}}{U_0} \sim \pm 1\% \quad . \qquad (64c)$$

## 2. Averaging intervals

The time averaging intervals required to establish an accept-

ably accurate estimate of the mean velocity will, in practical situations, be determined by the characteristics of two aspects of the flow, namely

(i) amplitude and temporal properties of the velocity fluctuations in the wake,

and

(ii) turbulence spectrum and intensity of the test section free stream.

The temporal properties of the velocity fluctuations in the wake are dominated by the vortex shedding mechanism. For a cylinder at $Re > 40$, the dimensionless vortex shedding frequency, or Strouhal number, $S$, is given by (Roshko 1954),

$$S \equiv \frac{d}{T_v U_\infty} \simeq 0.21 \tag{65}$$

where $T_v^{-1}$ is the vortex shedding frequency. To estimate the length $T_a$ of the time averaging interval required for a given accuracy, we must compute the variance of the mean velocity estimator

$$\tilde{u}(T_a) \equiv \frac{1}{T_a} \int_0^{T_a} u(t)\, dt \quad . \tag{66}$$

Note that, for long averaging intervals, we have

$$\lim_{T_a \to \infty} \left\{ \tilde{u}(T_a) \right\} \equiv \bar{u} \quad .$$

Now the variance of $\tilde{u}(T_a)$ is given by,

$$\text{var}\left\{\tilde{u}(T_a)\right\} = E\left\{\left[\tilde{u}(T_a) - \overline{u}\right]^2\right\}$$

$$= E\left\{\left[\tilde{u}(T_a)\right]^2\right\} - \overline{u}^2, \qquad (67)$$

where $E$ is the expectation operator. Substituting for $\tilde{u}(T_a)$, we have, after a little algebra

$$\text{var}\left\{\tilde{u}(T_a)\right\} = \frac{2}{T_a}\int_0^{T_a}\left(1 - \frac{\tau}{T_a}\right) R_u(\tau)\, d\tau \qquad (68)$$

where $R_u(\tau)$ is the autocorrelation function,

$$R_u(\tau) \equiv \overline{u'(t)\, u'(t+\tau)} \quad . \qquad (69)$$

of the velocity fluctuations.

We can approximate the autocorrelation function by assuming that the velocity fluctuations due to the vortices in the wake are uncoupled from the free stream turbulence, i.e.

$$R_u(\tau) \sim \overline{u'^2}(x,y)\; e^{-\tau/mT_v} \cos\left(2\pi \frac{\tau}{T_v}\right) + \overline{u_f'^2}\; e^{-\gamma\tau} \quad , \qquad (70)$$

where $\overline{u'^2}(x,y)$ is the turbulence level due to the velocity fluctuations in the wake, $T_v$ is the vortex shedding period, $m$ is the number of vortex shedding periods that it takes to decrease the

wake autocorrelation amplitude to $1/e$, $\overline{u_f'^2}$ is the free stream turbulence level and $\gamma^{-1}$ is the correlation time of the free stream turbulence. Substituting equation 70 into equation 68 we have

$$\mathrm{var}\left\{\tilde{u}(T_a)\right\} \sim \left[\frac{\overline{u'^2}(x,y)\,T_v}{2\pi^2 m} + \frac{2\overline{u_f'^2}}{\gamma}\right]\frac{1}{T_a}, \qquad (71)$$

where we have assumed that $mT_v \ll T_a$, $(2\pi m)^{-2} \gg 1$ and $\gamma^{-1} \ll T_a$. Consequently, the relative error in determining the mean velocity after an averaging interval $T_a$, is given by

$$\frac{\delta\bar{u}}{u_0(x)} \sim \left[\left(\frac{T_v}{2\pi^2 m T_a}\right)\frac{\overline{u'^2}(x,y)}{u_0^2(x)} + \left(\frac{2}{\gamma T_a}\right)\frac{\overline{u_f'^2}}{u_0^2(x)}\right]^{\frac{1}{2}}. \qquad (72)$$

Using equation 72, we can estimate the required averaging interval $T_a$, for a required relative error $\delta\bar{u}/u_0(x)$. Several conclusions can be drawn from equation 72.

(i) The required averaging interval decreases with the vortex shedding period. Consequently, *for a given Reynolds number, smaller diameters are to be preferred over large ones and air is preferrable to water as a working fluid.*

(ii) The required averaging interval is considerably shorter at the wake edges, where $\overline{u'^2}(x,y)/u_0^2(x)$ is small.

(iii) The free stream turbulence level should be small and it should have no low frequency components, i.e.

$$\overline{u_f'^2}/u_0^2(x) \ll 1 \qquad (73)$$

and

$$\gamma T_v/m << 1 \ . \tag{74}$$

It should be mentioned that unless the free stream velocity is monitored in real time, and recorded with the velocity data in the wake, *no drift in the free stream velocity can be tolerated, during the time it takes to traverse the wake,* at least not larger than the accuracy with which the mean velocity must be determined with respect to $U_0$ ($\lesssim 0.1\%$).

## 3. Flow uniformity requirements

The free stream mean velocity outside the wake should be sufficiently uniform to permit an accurate determination of $U_0$, as it enters in equation 42. An error $\delta U_0$ in determining $U_0$ will result in an error for $c_D$ of the order of

$$\delta c_D \sim 2 \frac{\delta U_0}{U_0} \left( \frac{h}{d} \right). \tag{75}$$

By way of example a 3% measurement maximum error of the drag coefficient due to this difficulty, for a $d \sim 0.5''$ in a $h \sim 20''$ test section requires that

$$\frac{\delta U_0}{U_0} \lesssim \tfrac{1}{2} \left( \frac{d}{h} \right) \delta c_D < 0.04\% \tag{76}$$

*It is anticipated that this will be one of the main sources of error in the final determination of the drag coefficient.*

## 4. Positioning requirements

The small cable diameters that are of interest here, namely

$$0.125'' \leq d \leq 4'' ,$$

necessitate that the positioning mechanism be capable of scanning the y-axis *in steps of at most 0.005".* The requirements for the z-axis will be dictated by the spanwise period of the structure of the cable under examination. It should be possible to position the measurement point at *ten stations within the spanwise period of the cable.* The requirements for measuring the streamwise coordinate are not very strict, as that quantity does not enter in the calculation of $c_D$ (equation 42). It would be desirable, however, to know the distance from the cable to within $\pm d$ for documentation purposes and also because *it might be possible to use the similarity properties of the wake, e.g. equations 54, 61, 62 and 63 and estimate* $c_D$ *by extrapolating to* $x/d \to \infty$ *the measurements of the first and third terms only, of equation 42, which only require that the mean streamwise velocity be measured.*

# V. Laser Doppler velocimetry

## 1. General considerations

The high accuracy required by the velocity measurements suggest laser Doppler velocimetry as the recommended method for determining the quantities of interest. The system should be designed to measure $\overline{u}$, $\overline{u'^2}$ and $\overline{v^2}$ to the accuracies specified by equation 64.

A variety of systems can perform such a task, ranging in cost by an order of magnitude, at least. The system that will be described here is a "barebones" system that can perform these measurements. Such a system, however, is labor intensive and whether it is the optimal final configuration depends on the anticipated volume of testing. The trade-off is between labor expense versus instrumentation automation, complexity and cost. It is not possible as of this writing, to explore the optimal system on the basis of cost effectiveness.

The "barebones" system should be able to yield measurements of the streamwise component $u$, as well as

$$u_+ = \frac{1}{\sqrt{2}} (u + v) \tag{77a}$$

and

$$u_- = \frac{1}{\sqrt{2}} (u - v). \tag{77b}$$

The data can best be derived from discrete particle measurements of

the corresponding velocity, i.e.

$$\left\{(u_i),\ i = 1,\ N\right\} \tag{78a}$$

$$\left\{(u_{+j}),\ j = 1,\ N_+\right\} \tag{78b}$$

$$\left\{(u_{-k}),\ k = 1,\ N_-\right\} \tag{78c}$$

at each measurement location.

From these data, it is possible to compute the quantities of interest, namely

$$\overline{u} = \langle u \rangle \tag{79a}$$

$$\overline{u'^2} = \langle u^2 \rangle - \langle u \rangle^2 \tag{79b}$$

$$\overline{v^2} = \langle u_+^2 \rangle + \langle u_-^2 \rangle - \langle u \rangle^2 \ , \tag{79c}$$

where the angle brackets denote ensemble averages, i.e.

$$\langle u \rangle = \frac{1}{N} \sum_i u_i \tag{80a}$$

$$\langle u^2 \rangle = \frac{1}{N} \sum_i u_i^2 \tag{80b}$$

$$\langle u_+^2 \rangle = \frac{1}{N_+} \sum_j u_{+j}^2 \tag{80c}$$

$$\langle u_-^2 \rangle = \frac{1}{N_-} \sum_k u_{-k}^2 \ . \tag{80d}$$

In computing the various terms of equations 79 and 80, care must be

exercised to carry a sufficient number of significant figures so as to be able to compute reliably the differences of the large, and almost equal, numbers that are required.

Problems due to laser Doppler sampling bias (Dimotakis 1976) are not expected to arise in the far wake, since the velocity measurements will always be close to the free stream velocity outside the wake, $U_0$ (or $U_0/\sqrt{2}$ for $u_+$ and $u_-$).

## 2. Optical arrangement

The envisaged optical system utilizes the LDV dual (forward) scatter mode. The velocity component selection can be implemented by generating *three* parallel beams, of equal intensity, which are incident on the transmitting lens. These should be located, as closely as possible, on the vertices of a right isosceles triangle whose hypotenuse is aligned with the streamwise vector and whose three vertices are on a radius from the optical center of the lens (see figure 4). A mechanical device (e.g. a reed mounted on a stepping rotary relay) can be employed to block one of the beams at a time, so that in any one configuration, two beams are transmitted which intersect at the common focal point (recall that the three beams are parallel) and selecting the corresponding velocity component.

A single, large aperture ($3 < f\# < 5$) collecting lens can image the common focal point of the transmitting system through an appropriately sized pinhole and on a photodetector. See figure 4. *The whole optical system should be so connected mechanically as to*

*minimize differential vibrations between the transmitting and collecting optics platforms.*

It could be argued that a backscatter arrangement would be simpler, in this case, obviating the collection optics lens and separate platform. I believe, however, that the disadvantages the backscatter system, namely

(i) loss of signal of two orders of magnitude,

(ii) sensitivity to window scattering,

requiring a 0.5 W laser (versus 5 mW which should be adequate for the forward scatter system) and high quality windows to minimize window scattering, render this choice a less desirable one.

We can summarize the optical requirements as follows:

(i) The three beams should be aligned before the transmitting lens so as to have a common crossing point in pairs.

(ii) The divergence of the three beams, before the transmitting lens, should be such as to ensure that the beams *focus and cross* at the same region in space. If this is not the case, the fringes in the focal volume will not be parallel and equidistant, resulting in an apparent spread $\delta u_{opt.}$ of the velocity distribution that will, in general, be indistinguishable from turbulent fluctuations.

(iii) If the dual forward scatter LDV mode is used, the optical requirements on the windows are rather lenient. Generally speaking it should be possible to have an undistorted view through them to avoid beam bending away

from the common focus, and sufficiently smooth to avoid diffuse scattering from the surfaces which will raise the shot noise level at the photodetector.

## 3. Signal processing

The output from the photodetector (photomultiplier tube, or avalanche photodiode + transimpedance amplifier) is amplified in a low-noise preamplifier and band-pass filtered, to eliminate frequencies outside the range of the Doppler frequencies that the signal can assume. The filtered signal is then processed by a counter type processor (DISA , TSI or GALCIT Mk IV) to yield the time of flight $\Delta t_i$, of the $i^{th}$ particle for $n_i$ fringes. The velocity is then given by

$$u_i = s \frac{n_i}{\Delta t_i} , \tag{81}$$

where $s$ is the fringe spacing

$$s = \frac{\lambda}{2 \sin \frac{\theta}{2}} , \tag{82}$$

and where $\lambda$ is the laser wavelength and $\theta$ the angle between the intersecting beams.

Generally speaking the signal processing system should have the following capabilities:

(i) It should be capable of measuring the Doppler frequencies $\nu_D$ anticipated in this experiment. In

particular, $\nu_D$ is given by

$$\nu_D = \frac{u_\perp}{s} , \tag{83}$$

where $u_\perp$ is the velocity component perpendicular to the fringe planes and $s$ is the fringe spacing (equation 82). Generally speaking, for most laboratory situations and common laser wavelengths (see equation 83),

$$1/s \sim 1 \text{ kHz} / (\text{cm/sec}).$$

With water as the fluid medium (see abscissa of figure 2), the range of Doppler frequencies is then

$$\sim 1 \text{ kHz} < (\nu_D)_{water} < \sim 300 \text{ kHz} \tag{85a}$$

and for air

$$\sim 15 \text{ kHz} < (\nu_D)_{air} < \sim 1.5 \text{ MHz}. \tag{85b}$$

(ii) The analog signal handling electronics (preamplifiers, bandpass filters, etc.) should be such as not to further degrade the signal-to-noise ratio due to the unavoidable photodetection shot noise. Since the latter contributes a signal-to-noise (power) ratio that decreases inversely as the signal bandwidth, we have

$$(S/N)_{shot} \propto 1/BW \propto 1/\nu_D \propto 1/u . \tag{86}$$

Consequently, this is more of a problem at the high velocities than at the low. This problem can be offset with higher laser powers, since we also have

$$(S/N)_{shot} \propto P_L \quad . \tag{87}$$

The effect of noise on the analog signal is to render the zero crossings of the Doppler burst less well defined, resulting in an uncertainty in the measurement of the time of flight $\Delta t_i$ , and an uncertainty $\delta u_{noise}$ in the velocity measurement.

(iii) The clock period that is utilized by the time of flight counter that determines $\Delta t_i$ (equation 81) must be sufficiently small so as not to be the resolution determining factor. If $\tau_c$ is the clock period, the apparent spread in the velocity distribution due to finite time of flight measurement resolution is given by

$$\delta u_{clock} = \frac{\tau_c}{\Delta t_i} u_i \quad , \tag{88}$$

or, using equation 81,

$$\delta u_{clock} = \frac{\tau_c}{s n_i} u_i^2 \quad , \tag{89}$$

where $n_i$ is the number of fringes that are utilized in the measurement. Evidently, the problem becomes more severe as the velocity increases but is not expected to

to be an important one considering the capabilities of presently available processors ($\tau_c \sim 10^{-8}$ sec).

To the extent that the three sources of error are independent:

$$\text{optical imperfections} \rightarrow \delta u_{\text{opt.}}$$
$$\text{shot \& electronic noise} \rightarrow \delta u_{\text{noise}}$$
$$\text{finite clock period} \rightarrow \delta u_{\text{clock}} ,$$

their variances add, yielding an instrumental width $\delta u_{\text{instr.}}$ given by,

$$\delta u_{\text{instr.}} = \left( \delta u^2_{\text{opt.}} + \delta u^2_{\text{noise}} + \delta u^2_{\text{clock}} \right)^{\frac{1}{2}} . \qquad (90)$$

This instrumental width is indistinguishable from the spread in the velocity distribution due to turbulent fluctuations (unless spectra are computed in which case it appears as a base line background white noise level). Consequently the measured mean square fluctuation is given by,

$$\overline{u'^2}_{\text{meas.}} \simeq \overline{u'^2}_{\text{turb.}} + \delta u^2_{\text{instr.}} . \qquad (91)$$

If we include this effect in the calculation of the expected accuracy for the mean velocity after an averaging interval $T_a$, we have (see equation 72),

$$\frac{\delta\bar{u}}{u_0(x)} \simeq \left[\left(\frac{T_v}{2\pi^2 m T_a}\right)\frac{\overline{u'^2}(x,y)}{u_0^2(x)} + \left(\frac{2}{\gamma T_a}\right)\frac{\overline{u_f'^2}}{u_0^2(x)} + \left(\frac{\tau_s}{T_a}\right)\frac{\delta u^2_{instr.}}{u_0^2(x)}\right]^{\frac{1}{2}} \qquad (92)$$

where $\tau_s$ is the mean time between velocity samples ($\tau_s^{-1} \equiv$ data rate).

It should be noted that, *whereas the accuracy in determining the mean velocity can always be improved by a long averaging interval (equation 92), the mean square fluctuation measurement will, at best, be given by equation 91.* It should be noted that even though $\delta u^2_{instr.}$ can be subtracted from the measured mean square fluctuation (by measuring it, for example, outside the wake) it is desirable to keep it as small as possible and, in this case in particular, consistent with the specifications of equation 64. By way of reference, moderately careful laser Doppler measurements to date at the GALCIT Free Surface Water Tunnel have achieved

$$\frac{\delta u_{instr.}}{u} \lesssim 0.5\% \ .$$

(There is no reason to believe that this could not be improved, should the need arise, by almost an order of magnitude.)

## 4. Data acquisition

The data rate should be controlled so that a sufficient number

of velocity samples is recorded during the averaging interval $T_a$. This will generally require an automated data acquisition system that can record the (digital) time of flight $\Delta t_i$ (and the number of fringes $n_i$, if required) for each particle. This can be on magnetic tape, with subsequent computer data reduction, or an on-line computer, if real time data reduction is found to be necessary.

## 4. Fluid medium

Almost any fluid can be used to perform this measurement. The low velocities that would have to be utilized in water ($u > 1$ cm/sec) do not present a measurement problem ($\sim$ 2 mm/sec have been measured by the author at the GALCIT Free Surface Water Tunnel). Correspondingly, the higher velocities that would have to be utilized in air ($u < 45$ m/sec) do not present a problem either ($\sim$ 500 m/sec have been measured by the author in the JPL 20" supersonic tunnel, with accuracies that meet the present specifications). The main difference, as far as the laser Doppler velocity measurement is concerned, is that air has to be seeded uniformly with appropriate scattering particles. While this is not difficult in a closed circuit wind tunnel, *it is a major undertaking to do well in an open circuit wind tunnel without compromising the flow quality*. Consequently, it can be seen that the deciding considerations are not dictated by the velocity measurements, but by relevant features of the candidate test facility. In particular,

(i) flow quality in the test section (see section IV.3), and

(ii) accessibility from both sides of the test section,

through windows of adequate size and quality (see section V.2).

## VI. Suggested program

The proposed method of drag coefficient measurement is relatively straightforward and likely to yield, with adequate care, accuracies quite a bit better than the ±5% specification goal. It would be wise, however, at this stage, to conduct a pilot calibration program using a cylinder whose drag coefficient is accurately known throughout the range of Reynolds numbers of interest. To conduct such a program, a test facility should be chosen which either meets the flow quality specifications, or can easily be modified to that effect.

It would be inadvisable, in my opinion, to start from scratch and design or purchase the LDV laser, optics, positioning, signal processing, data acquisition and data processing system. A rough figure for such a system, including the man hours to design and assemble it, would be approximately $100,000. It would be preferable to rely heavily on existing equipment for the proof-of-concept program and decide, from its results and the anticipated test program size, on an optimal instrumentation package that will perform the specified task.

# REFERENCES

1. P. E. DIMOTAKIS (1976), "Single scattering particle laser-Doppler measurements of turbulence." *AGARD Symp. Non-Instrumentation in Fluid Flow Res., Saint-Louis, France,* paper 10.

2. A. ROSHKO (1954), *On the development of turbulent wakes from vortex streets,* NACA Rep. 1191.

3. H. SCHLICHTING (1968), *Boundary Layer Theory,* (McGraw-Hill, Sixth Ed.), p. 692.

4. A. A. TOWNSEND (1976), *The Structure of Turbulent Shear Flow* (Cambridge Univ. Press), pp. 188-232.

## Appendix 1. Useful numbers and units.

1. Properties of air at 22°C (71°F), 1 Atm.

$\rho = 1.197\times10^{-3}$ g/cm$^3$

$\mu = 1.822\times10^{-4}$ g/cm•sec

$\nu = \mu/\rho = 0.152$ cm$^2$/sec

$\rho\nu^2 = 2.77\times10^{-5}$ g•cm/sec$^2$

2. Properties of water at 22°C (71°F), 1 Atm.

$\rho = 0.9978$ g/cm$^3$

$\mu = 0.9548\times10^{-2}$ g/cm•sec

$\nu = \mu/\rho = 0.957\times10^{-2}$ cm$^2$/sec

$\rho\nu^2 = 9.14\times10^{-5}$ g•cm/sec$^2$

3. Units of pressure

1 dyne/cm$^2$ = $7.50\times10^{-4}$ mmHg (0°C)

= $4.01\times10^{-4}$ in H (4°C)

= $1.45\times10^{-5}$ lbs/sq.in

4. Units of velocity

1 cm/sec = $1.00\times10^{-2}$ m/sec

= $3.28\times10^{-2}$ ft/sec

= $1.94\times10^{-2}$ knots.

1 knot = 51.4 cm/sec

= 1.69 ft/sec

= 0.514 m/sec.

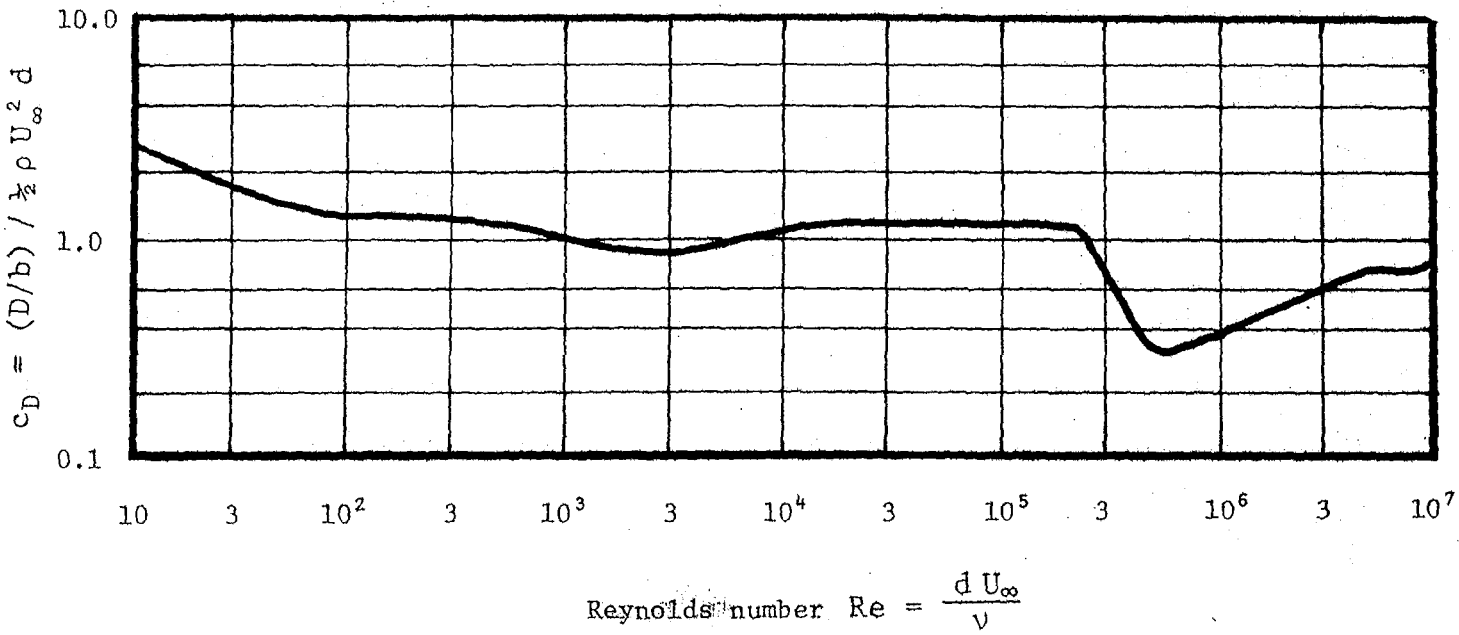


FIGURE 1. Cylinder drag coefficient as a function of Reynolds number.

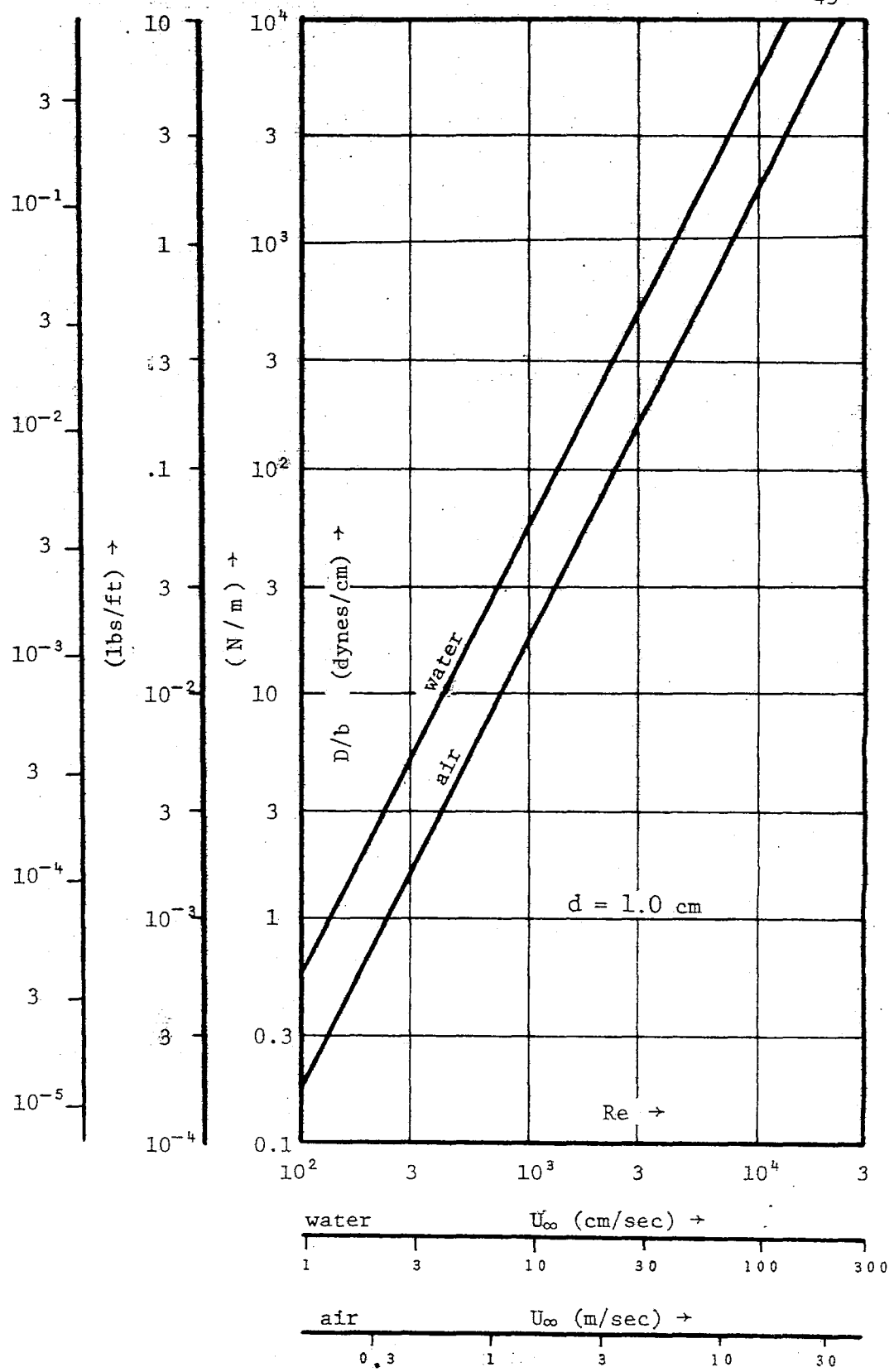


FIGURE 2. 1 cm diameter cylinder drag per unit span, in water and air for a drag coefficient of $C_D \sim 1.2$

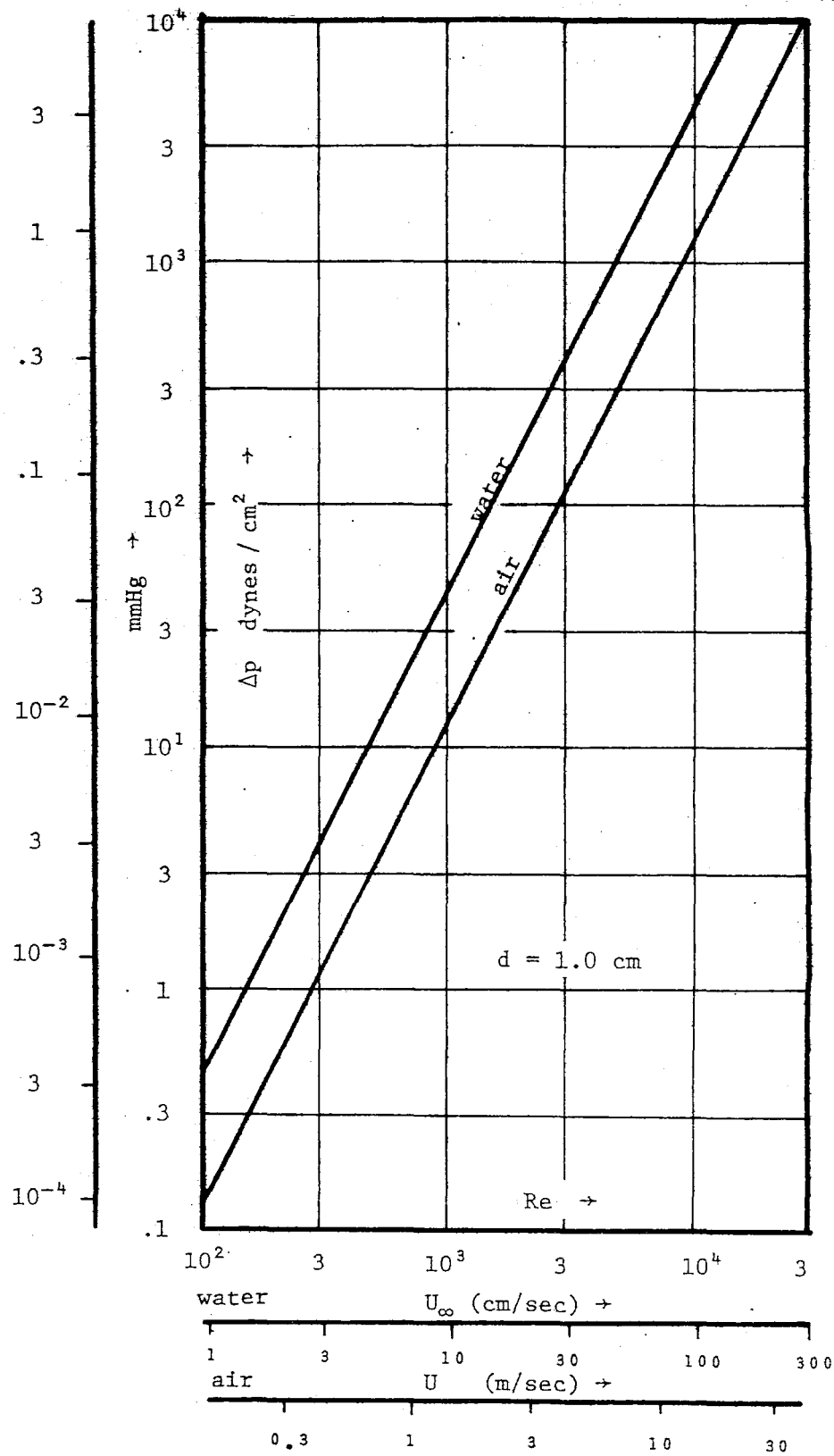


FIGURE 3. Pressures on a 1 cm diameter cylinder, in water and air, for a pressure coefficient of $c_p \sim 1$ .

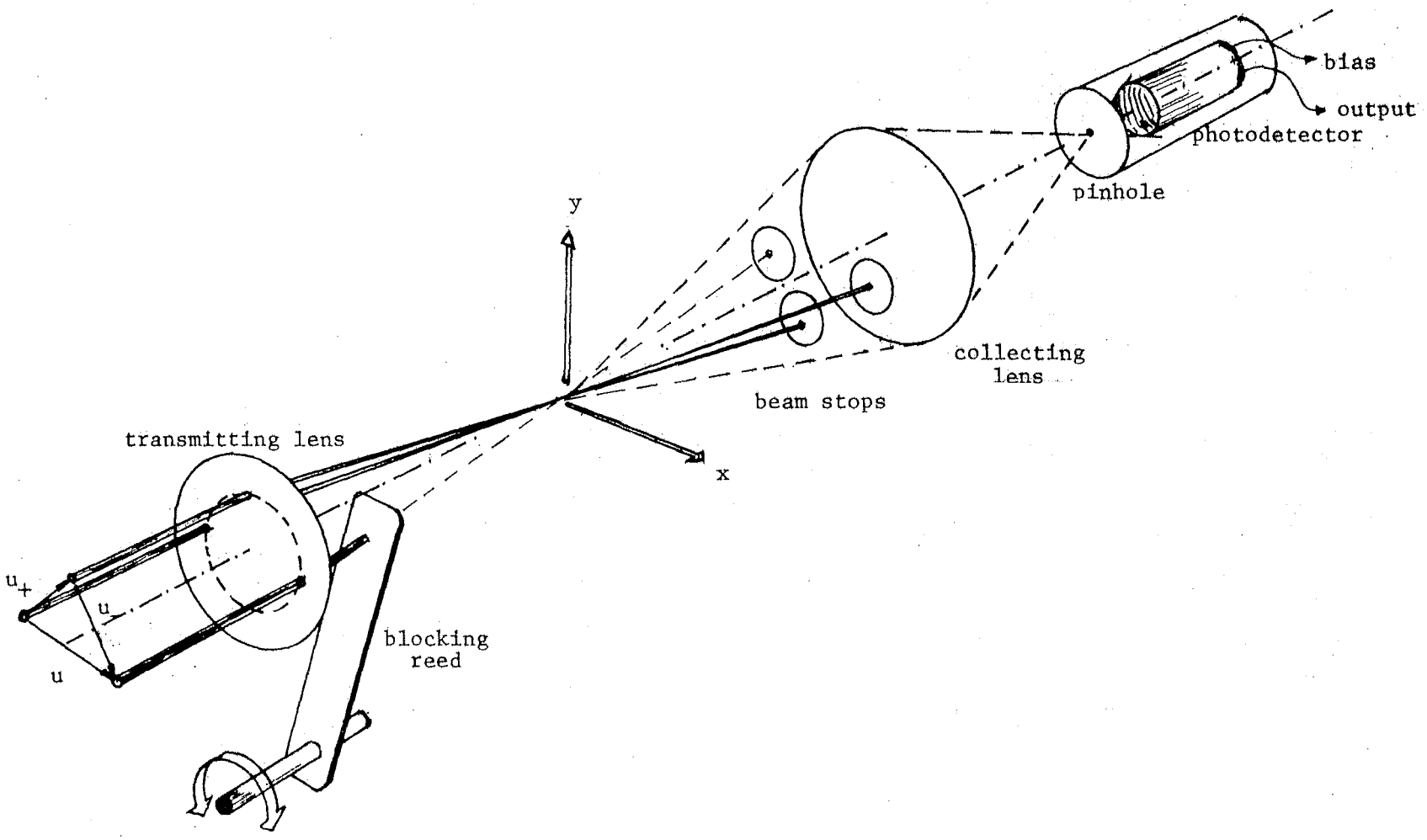


FIGURE 4. Optical arrangement. Shown configured for $(u + v) / \sqrt{2}$ measurement.